RESEARCH ARTICLE

Upregulation of Mitochondrial Content in Cytochrome *c* Oxidase Deficient Fibroblasts

Aviram Kogot-Levin[1], Ann Saada[2], Gil Leibowitz[1], Devorah Soiferman[2], Liza Douiev[2], Itamar Raz[1], Sarah Weksler-Zangen[1]*

1 The Diabetes Unit, Department of Internal Medicine, Hadassah-Hebrew University Medical Center, Jerusalem, Israel, 2 Monique and Jacques Roboh Department of Genetic Research and Department of Genetic and Metabolic Diseases, Hadassah-Hebrew University Medical Center, Jerusalem, Israel

* sarahz@hadassah.org.il

Abstract

Cytochrome-c-oxidase (COX) deficiency is a frequent cause of mitochondrial disease and is associated with a wide spectrum of clinical phenotypes. We studied mitochondrial function and biogenesis in fibroblasts derived from the Cohen (CDs) rat, an animal model of COX deficiency. COX activity in CDs-fibroblasts was 50% reduced compared to control rat fibroblasts (P<0.01). ROS-production in CDs fibroblasts increased, along with marked mitochondrial fragmentation and decreased mitochondrial membrane-potential, indicating mitochondrial dysfunction. Surprisingly, cellular ATP content, oxygen consumption rate (OCR) and the extracellular acidification rate (ECAR) were unchanged. To clarify the discrepancy between mitochondrial dysfunction and ATP production, we studied mitochondrial biogenesis and turnover. The content of mitochondria was higher in CDs-fibroblasts. Consistently, AMPK activity and the expression of NRF1-target genes, NRF2 and PGC1-α that mediate mitochondrial biogenesis were increased (P<0.01 vs control fibroblast). In CDs-fibrobalsts, the number of autophagosomes (LC3+ puncta) containing mitochondria in CDs fibroblasts was similar to that in control fibroblasts, suggesting that mitophagy was intact. Altogether, our findings demonstrate that mitochondrial dysfunction and oxidative stress are associated with an increase in mitochondrial biogenesis, resulting in preservation of ATP generation.

Introduction

Cytochrome *c* oxidase (COX, complex IV) is the last enzyme of the mitochondrial respiratory chain and is a regulation site for mitochondrial oxidative phosphorylation (OXPHOS) system. COX catalyzes the transfer of electrons from reduced cytochrome *c* to molecular oxygen [1,2] in a reaction coupled to proton pumping across the inner mitochondrial-membrane, thereby assisting the establishment of the mitochondrial electrochemical gradient [3].

COX deficiency in humans is a commonly recognized cause of mitochondrial disorder [4]. In addition, alteration of COX function was demonstrated in a diverse array of pathological conditions such as Alzheimer's and Parkinson's diseases, and age related loss of COX activity was also

reported [5,6]. For diagnostic testing, cultured skin fibroblasts are an attractive tissue to evaluate OXPHOS function because of the minimally invasive character of sampling and the amount of cell material obtained by culturing [7]. Studies in human COX-deficient fibroblasts, derived from patients, have revealed diminished COX activity, compromised ATP production, reactive oxygen species (ROS) overproduction and abnormal mitochondrial morphology [8–10].

The Cohen rat (CDs) is an inbred genetic model of COX deficiency [11–13] exhibiting partially reduced COX activity in different tissues. The CDs rats demonstrate no overt pathology but presents reduced pregnancy and fertility rate, increased embryonic mortality and lower body weight [14]. Previous studies in the CDs model have shown that a severe COX impairment in pancreatic-islets induced by high-sucrose low-copper diet was associated with diabetes development [11,13]. We recently showed that islets isolated from CDs rats exhibited a consistent partial reduction in COX activity, ATP content and glucose stimulated insulin secretion, which could be recovered by feeding on a copper-sufficient diabetogenic-diet. These observations are supporting the involvement of COX in β-cell dysfunction in CDs rat islets [12].

Since COX-deficiency is ubiquitous, primary fibroblasts provide a useful tool to study the CDs mitochondrial phenotype. In this study, we examine the association between COX-deficiency and mitochondrial biogenesis in the CDs-fibroblasts.

Methods

Cell culture

Fibroblasts were obtained from rat ear biopsies of CDs and control Cohen diabetes-resistant (CDr) rats fed regular chow-diet (Teklad, Harlan Laboratories, USA). The control CDr strain is genetically derived experimental model that maintains normoglycemia on the regular diet and the diabetogenic high sucrose low copper diet [11]. Fibroblasts were cultured in DMEM medium containing glucose (4.5 g/L), 10% fetal calf serum (FCS) and 100 IU/mL penicillin/streptomycin (DMEM-Glu) (All from Biological Industries, Kibbutz Beit Haemek, Israel) at 37°C, 5% CO_2. The DMEM-Glu culture medium was used for all experiments unless otherwise stated. To induce starvation, fibroblasts were washed with phosphate-buffered saline (PBS) and incubated in glucose-free DMEM without fetal calf serum. For autophagy analysis, cells were incubated with or without 100 nM of bafilomycin A1 for 4 h.

Enzymatic activities of cytochrome *c* oxidase and citrate synthase

Enzymatic activities of COX and of citrate synthase (CS), a mitochondrial control enzyme, were determined in cell or tissue homogenates by standard spectrophotometric methods as previously described [15]. Briefly, COX activity was measured by following the oxidation of reduced cytochrome *c* at 550 nm. CS activity was measured in the presence of acetyl-CoA and oxaloacetate by monitoring the release of CoASH coupled to 5′5-dithiobis (2-nitrobenzoic) acid at 412 nm. COX activity was expressed as a ratio normalized to that of CS.

Assays

For the different assays 2000 cells/well were seeded in quadruplicate on four 96-well cell culture plates as we have previously described [16]. The following day, medium was removed and replaced with 100 µl of fresh DMEM-Glu permissive medium or a restrictive glucose-free medium (Biological Industries, Kibbutz Beit Haemek, Israel) supplemented with 10% dialyzed FCS, 5 mM galactose, 2 mM l-glutamine and 100 IU/mL penicillin/streptomycin (DMEM--Gal). Following 72 h, tissue cultures were analyzed for cell biomass, ROS, ATP, membrane potential and mitochondrial content.

Cell biomass was measured by a colorimetric method using methylene blue (MB) as described [16]. Cells were fixed with 0.5% glutaraldehyde for 10 min, rinsed with water, stained with 1% MB in 0.1 M borate buffer for 1 h, rinsed with water and allowed to dry. The dye was extracted from the cells using 0.1 N HCl at 37°C for 1 h and then measured at A_{620} nm.

Intracellular ROS production was measured using 2′,7′-dichlorodihydrofluorescein diacetate (DCF) (Biotium, Harvard, CA, USA) [17]. Briefly, growth medium was removed and replaced with 100 μl of 10 μM DCF in PBS-Ca^{2+} Mg^{2+} (PBS containing 0.9 mM $CaCl_2$ and 0.5 mM $MgCl_2$) and incubated for 25 min at 37°C, 5% CO2. DCF was replaced with 100 μl PBS-Ca^{2+} Mg^{2+} and ROS production was monitored for 20 min at λex 485 nm, λem 520 nm.

ATP level was quantified by the ATPlite® luciferin-luciferase bioluminescence assay according to the manufacturer's instructions (Perkin Elmer Waltham MA, USA).

Mitochondrial content and mitochondrial membrane potential were estimated, respectively, using MitoTracker Green FM (MTG) and tetramethylrhodamine ethyl ester (TMRE) (Molecular Probes, Eugene, OR, USA). MitoTracker Green was added to the existing medium to a final concentration of 200 nM and cells were incubated for 45 min at 37°C, 5% CO_2. TMRE was added successively to a final concentration of 50 nM and the cells were incubated for an additional 45 min at 37°C, 5% CO_2. Medium was removed and after rinsing once with PBS, replaced with 100 μl PBS. The plate was read at 37°C, λ_{ex} 485 nm, λ_{em} 528 nm (MTG) and λ_{ex} 485 nm, λ_{em} 590 nm (TMRE).

Absorbance, fluorescence and luminescence measurements were performed using a Synergy HT microplate reader (Bio-Tek Instruments, Vinoosky, VT, USA) at 30°C unless otherwise specified. Relative fluorescence units (RFU) and relative luminescence units (RLU) were calculated by normalizing to cell biomass as measured by MB.

Fluorescence microscopy

Fibroblasts were grown in DMEM-Glu and stained with 250 nM MitoTracker Red CMXRos (Invitrogen). Cells were examined with a confocal microscope (40×/100×) (Olympus BX-UCB). All micrographs were taken under the same conditions and the fluorescence intensity of the mitochondria relative to the cell volume was calculated in 200 cells using the ImageJ software (NIH, Bethesda, MD).

Immunofluorescence staining

Fibroblasts grown on glass coverslips were incubated with 2 μM MitoTracker Red CMXRos (Invitrogen) for 45 min at 37°C, 5% CO2. Cells were washed in PBS and fixed with 4% paraformaldehyde for 15 min and then permeabilized for 10 min with 0.3% Triton X-100. Following, blocking was performed with 2.5% bovine serum albumin in PBS for 30 min. Subsequently, cells were incubated with primary antibodies directed against LC3B (microtubule-associated protein 1 light chain-3B, Cell signaling) for 2 h at room temperature. After washing, they were incubated for 1 h at room temperature with Cy3-conjugated anti-rabbit secondary antibodies (Jackson ImmunoResearch Laboratories, West Grove, PA), washed, mounted on slides and examined with a confocal microscope (Olympus BX-UCB).

XF24 Seahorse Flux Analyzer

Oxygen consumption rate (OCR) and extra-cellular acidification rate (ECAR) were measured using an XF24 extracellular flux analyzer (Seahorse Biosciences). Fibroblasts were seeded in an XF 24-well cell culture plate (Seahorse Bioscience) at a density of 20×10^3 cells/well in 300 μl of DMEM-Glu medium and incubated for 24h at 37°C, 5% CO_2. The following day the medium was replaced with fresh DMEM-Glu. After 48hrs, the growth medium was changed to 500 μl of

unbuffered DMEM, pH 7.4, and cells were incubated at 37°C without CO_2 for 1h for equilibration before starting the assay. OCR and ECAR were measured simultaneously for ~3 min in repeated cycles, to obtain basal rates. After baseline measurements, OCR and maximal ECAR were measured after the injection of Oligomycin to a final concentration of 1 μM. Subsequently, Carbonyl cyanide-4-(trifluoromethoxy)phenylhydrazone (FCCP) was injected to reach a working concentration of 5 μM and the maximal OCR was measured. Non-mitochondrial oxygen consumption was measured after the injection of rotenone and Antimycin A to a final concentration of 3 μM each. All OCR and ECAR values were normalized to cell biomass measured by the methylene blue method.

Western blot analysis

Protein samples were electrophoresed on a 12% SDS-PAGE and transferred to a nitrocellulose-membrane. Blot was blocked and incubated with anti-COX1 (MitoSciences), anti-phospho-AMPKα-(Thr[172]) (phosphorylated adenosine monophosphate activated protein kinase, Cell signaling), phospho-ACC-(Ser[79]) (phospho-acetyl-CoA carboxylase, Cell signaling), PGC-1α (Peroxisome proliferator-activated receptor gamma coactivator 1-alpha, Abcam) or anti-LC3B (Cell signaling) antibodies overnight at 4°C. Membrane was washed and incubated with horseradish peroxidase-conjugated secondary antibody for 1 h at room temperature and bound antibodies were detected using the SuperSignal West Pico chemiluminescent substrate (Thermo Scientific, USA). Band densities were analyzed using the ImageJ software.

Real-time PCR

Total RNA was isolated from fibroblasts using Tri-Reagent (Telron, Israel). First-strand cDNA synthesis was performed using the High Capacity cDNA Reverse Transcription kit (Applied Biosystems). Real-time PCR (RT-PCR) was performed using Fast SYBR Green Master Mix (Applied Biosystems) and the ABI PRISM 7900HT sequence detection system (Applied Biosystems) with 10 ng cDNA. The thermal cycling parameters were: step 1, 95°C for 20 s; step 2, 95°C for 1 s; step 3, 60°C for 20 s. Step 2 was repeated for 40 cycles. Relative mRNA expression was calculated from the cycle threshold (Ct) values relative to β-glucuronidase (GUSB) for normalization and the results were expressed as the fold change of control fibroblasts. Primer sequences are listed in Table 1.

Protein determination

Protein concentration was determined by the Lowry method [18].

Table 1. Sequence of primers for RT-PCR.

Gene	Forward primer	Reverse primer
COX1	5'-TGGAGCCCCTGATATAGCATTC-3'	5'-CCAGCTTCTACTATGGAGGATGC-3'
COX2	5'-GCACAATAGACGCCCAAGAAG-3'	5'-AATTCGTAGGGAGGGAAGGG-3'
COX4	5'- TGAACAAGGGCACCAATGA-3'	5'- GCCATACACGTAGCTCTTCTC-3'
COX5b	5'-TCCATACAATATGCTACCTCCAAA-3'	5'-ACAGATGCAGCCCACTATTC-3'
COX10	5'-TTCCTCAAGCGCATGTATGT-3'	5'-GTGTGCTCAAGAAGAGGAGAAG-3'
COX17	5'-AGAAGCCTCTGAAGCCCTGC-3'	5'-GGCCTCGATGAGATGTCCACAG-3'
TFAM	5'-GCCTGTCAGCCTTATCTGTATT-3'	5'-TGCATCTGGGTGTTTAGCTTTA-3'
NRF1	5'-CTATCCGAAAGAGACAGCAGAC-3'	5'-GGGTGAGATGCAGAGAACAA-3'
NRF2	5'-CTGTGATCTGTCCCTGTGTAAA-3'	5'-GGACTTGTGTTCAGCGAAATG-3'
GUSB	5'-CAGGAGAGTGGTGTTGAGAATC-3'	5'-TGGTGATGTCAGCCTCAAAG-3'

Statistics

Statistical significance was assessed by two-tailed student t-test and one-way analysis of variance (ANOVA). A statistical-difference of p<0.05 was considered statistically significant.

Results

COX activity and mitochondrial morphology

We found decreased COX activity per citrate synthase activity (~50% of the control) in primary fibroblasts derived from the CDs-rats (Fig 1A; p<0.01). COX to CS activity was also reduced in liver, heart and isolated pancreatic-islets of CDs rats compared with age-matched control rats (Fig 1A; p<0.01), supporting the occurrence of a general COX deficiency in this rat model. COX activity per mg protein was also reduced in all tissues examined from the CDs, while CS activity was mostly unchanged relative to the control (Fig 1B & 1C; p<0.01). In CDs fibroblasts enzymatic activity of CS was slightly but significantly increased (Fig 1C; p<0.05). Moreover, Western blot analysis revealed reduced COX1 subunit protein levels in fibroblasts and tissues of the CDs rats (Fig 1D). To visualize mitochondria fibroblasts were stained with the mitochondria-specific dye MitoTracker Red. In control fibroblasts, mitochondria were organized in extended tubular structures (Fig 2A, upper panel), whereas, in the CDs fibroblasts, the mitochondria morphology was abnormal with rounded and fragmented appearance (Fig 2A, lower panel). The intensity of mitochondrial staining was markedly increased in fibroblasts of the CDs, which may suggest increased mitochondrial mass (Fig 2A, lower panel). Quantification of MitoTracker staining demonstrated an 80% increase in fluorescence intensity in the CDs compared to control fibroblasts confirming the possibility of an increased mitochondrial mass (Fig 2B; p<0.01).

Cell biomass, mitochondrial content, mitochondrial membrane potential, ATP content and ROS production

The fibroblasts were assessed for ROS production, ATP content, mitochondrial content and membrane potential. Cells were cultured in medium containing glucose that support glycolysis or a medium containing galactose, which does not support glycolysis thus forcing cells to rely on mitochondrial OXPHOS to produce ATP. We found the cell biomass of CDs and control fibroblasts was comparable on permissive DMEM-Glu. However, it was reduced by 35% in the restrictive medium DMEM-Gal that contains galactose as an energy source (Fig 3A; p<0.01 relative to the control fibroblasts). Mitochondrial content was assessed by the mitochondrial dye MitoTracker Green FM that binds mitochondrial membrane independent of the membrane potential, an accepted method to measure mitochondrial mass [19]. In accordance with our previous microscopic observations, we found mitochondrial content in fibroblasts of CDs to be increased by 50% on DMEM-Glu further increasing by 70% on DMEM-Gal, compared with the control (Fig 3B; p<0.01). The mitochondrial membrane potential of CDs-fibroblasts was reduced by 15% on DMEM-Glu and by 45% in and DMEM-Gal, relative to that of the control fibroblasts (Fig 3C; p<0.05). Surprisingly however, the total cellular ATP content of the CDs fibroblasts was comparable to that of the control in both culture media (Fig 3D). Yet, when normalized to mitochondrial content and not to cell biomass, ATP levels were reduced in the CDs fibroblasts (Fig 3E; p<0.01). Kinetic measurement of ROS production showed that the rate was markedly increased in the CDs fibroblasts on both media, but the increase in the DMEM-Gal was much higher (Fig 3F; p<0.01).
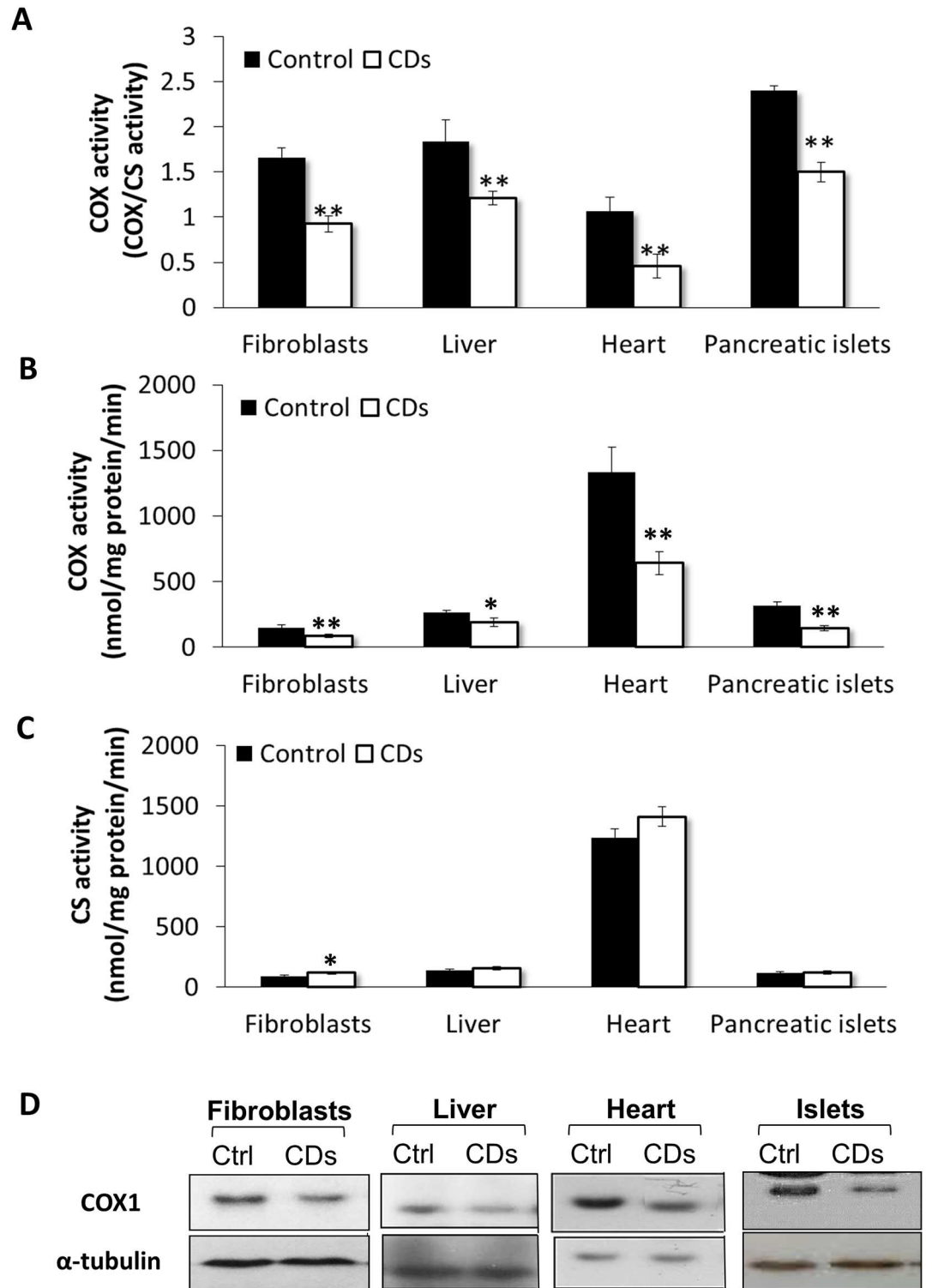
Fig 1. COX deficiency in the CDs rats. (A) COX activity normalized to citrate synthase (CS) activity in fibroblasts, liver, heart and pancreatic-islets of CDs and control rats. (B) COX activity per mg protein. (C) CS activity per mg protein. (D) Western-blot analysis of COX1. Values are mean ± S.E. of three independent experiments. *p<0.05, **p<0.01.

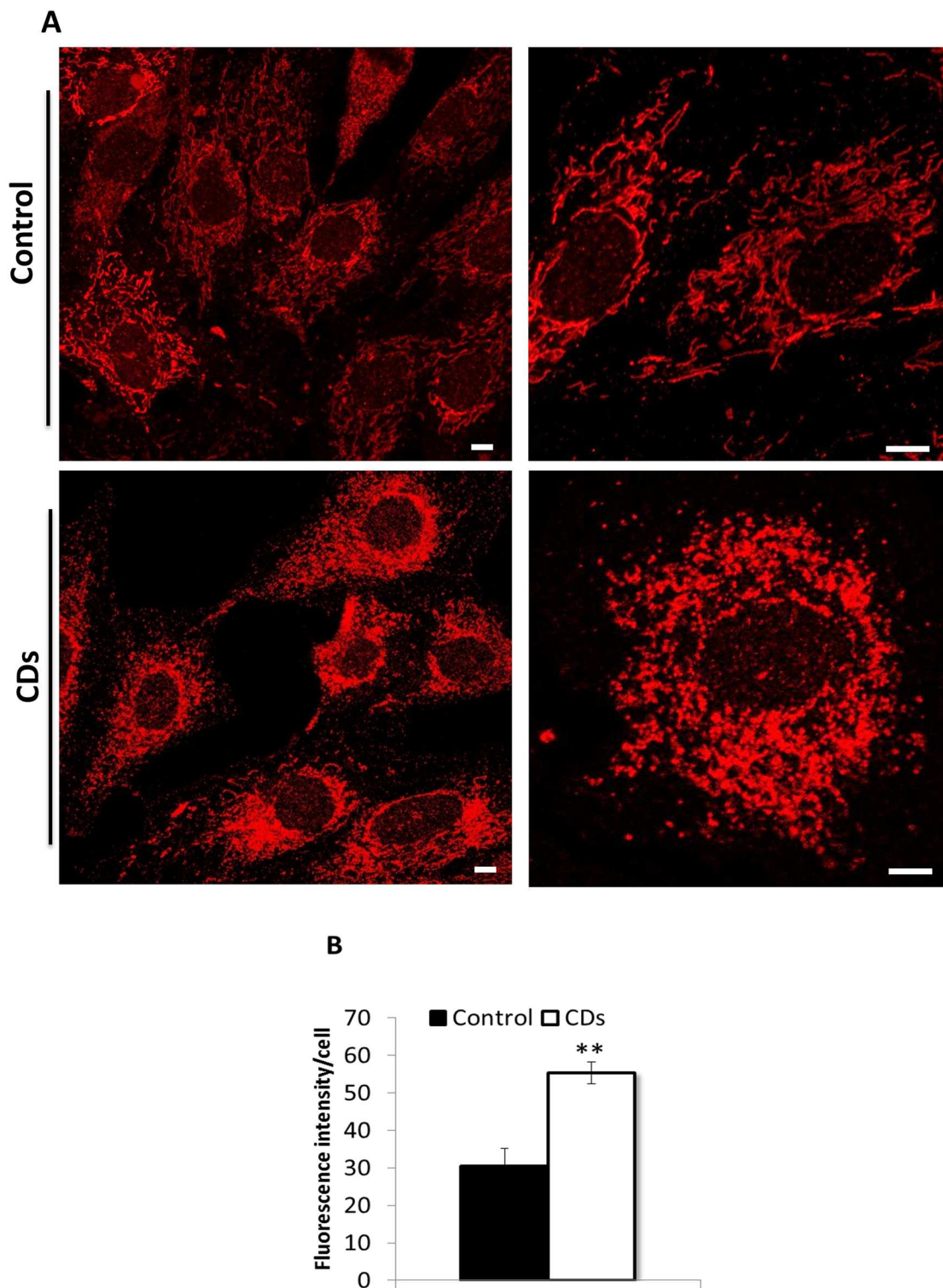doi:10.1371/journal.pone.0165417.g001

Fig 2. Mitochondrial morphology. (A) Representative confocal microscopy images of control (upper panel) and CDs fibroblasts (lower panel) stained with MitoTracker Red. (B) Quantification of MitoTracker Red fluorescence intensities per cell volume (n = 200 cells). Values are mean ± S.E. of three independent experiments. Scale bar, 10 μm. **p<0.01.

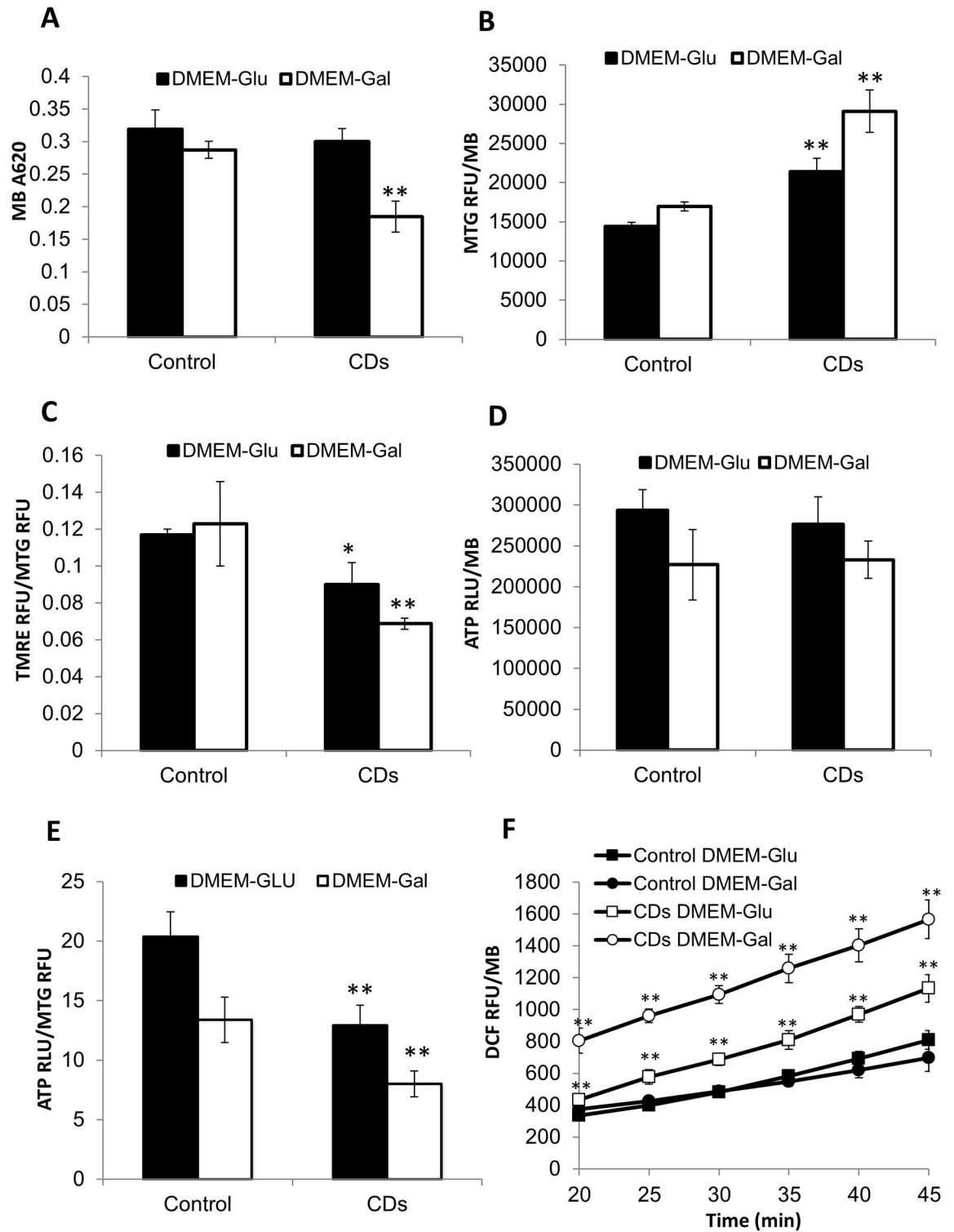doi:10.1371/journal.pone.0165417.g002

Fig 3. Cell biomass, mitochondrial content, mitochondrial membrane potential, ATP content and ROS production.
Fibroblasts were grown in either DMEM-Glu or DMEM-Gal and examined as described under materials and methods. (A)
Cell biomass. (B) Mitochondrial content measured by MTG. (C) Mitochondrial membrane potential. (D) Cellular ATP
content. (E) ATP content per mitochondria. (F) Kinetics of ROS production. Results are shown as normalized to cell
biomass measured by methylene blue (MB) and values are means ± S.E. RFU, relative fluorescence units; RLU, relative
luminescence units. (n = 3). *p<0.05, **p<0.01.

doi:10.1371/journal.pone.0165417.g003

—

Oxygen Consumption Rate (OCR) and Extracellular Acidification Rate (ECAR)

We further measured oxygen consumption rate (OCR) and extracellular Acidification Rate (ECAR) which are indicators of mitochondrial respiration and glycolysis respectively. Basal and maximal (stimulated by FCCP) OCR was similar in CDs and the control fibroblasts, suggesting intact mitochondrial respiration (Fig 4A). The basal and maximal (stimulated by Oligomycin) ECAR levels were also comparable in the CDs and control fibroblasts (Fig 4B). Moreover, the OCR/ECAR ratio was similar in the CDs and control fibroblasts, further suggesting no glycolytic shift in metabolism (Fig 4C).

Mitochondrial biogenesis

We analyzed the relative mRNA-expression of transcription factors affecting mitochondrial biogenesis TFAM, NRF1 and NRF2 [20]. We found the expression levels of TFAM and NRF1 which mediate mitochondrial biogenesis, was similar in the CDs and the control fibroblasts (Fig 5A). In contrast, the expression of NRF2, that facilitate cellular responses to oxidative stress, was increased by 60% in fibroblasts of CDs, supporting the occurrence of oxidative stress (Fig 5A; $p < 0.01$). Although the mRNA-expression of NRF1 and TFAM was unchanged, several of their downstream targets including COX subunits COX1, COX2, COX4 and COX5b as well as COX chaperones COX10 and COX17 were all upregulated in the CDs fibroblasts relative to the control (Fig 5B & 5C; $p < 0.05$), possibly indicating increased synthesis. To gain further insight into the possible mechanism underlying mitochondrial biogenesis in CDs we measured AMPK phosphorylation and activity, evident by the phosphorylation of its downstream target acetyl-CoA carboxylase (ACC) by western-blot. We observed increased pAMPK levels in the CDs fibroblasts compared with the control fibroblasts (Fig 5E; $p < 0.01$). In agreement, levels of pACC were significantly higher in the CDs fibroblasts (Fig 5E; $p < 0.01$). In addition, levels of PGC-1α, a transcriptional regulator for genes involved in mitochondrial biogenesis, were also increased in the CDs fibroblasts (Fig 5E; $p < 0.01$).

Mitophagy

We sought to examine the possibility that the increase in mitochondrial mass observed in the CDs fibroblasts is due to decreased mitochondrial clearance by autophagy. To study autophagy we assessed endogenous LC3-I and LC3-II by western-blotting. During autophagosome formation, the LC3-I isoform is converted into LC3-II, thus serving as a marker of autophagosomes number and the induction of autophagy [21,22]. When grown either in a complete media or under starvation conditions a comparable low LC3-II levels and LC3-II/LC3-I ratio could be detected in the CDs and the control fibroblasts (Fig 6). Autophagy inhibition by bafilomycin A1, that inhibits autolysosomal degradation [23], induced a significant and similar increase in LC3-II levels and the LC3-II/LC3-I ratio in the CDs and control fibroblasts, under both normal and starvation conditions (Fig 6), indicating normal autophagic flux. Since some mitochondrial defects increase specific degradation of mitochondria (mitophagy) [24], we analyzed the co-localization of Mitotracker Red with LC3, as an index of mitophagy, by confocal microscopy [25,26]. We observed LC3-positive structures in both the CDs and the control fibroblasts, with no apparent differences (Fig 7A). Moreover, LC3 co-localization with the mitochondria with or without Bafilomycin A1 was similar in the CDs and the control fibroblasts (Fig 7A). Further quantification of fluorescence intensity of LC3 signal co-localized with mitochondria (Mito-Tracker Red) showed no difference in co-localization per cell (Fig 7B), indicating no major autophagic mitochondrial sequestration.
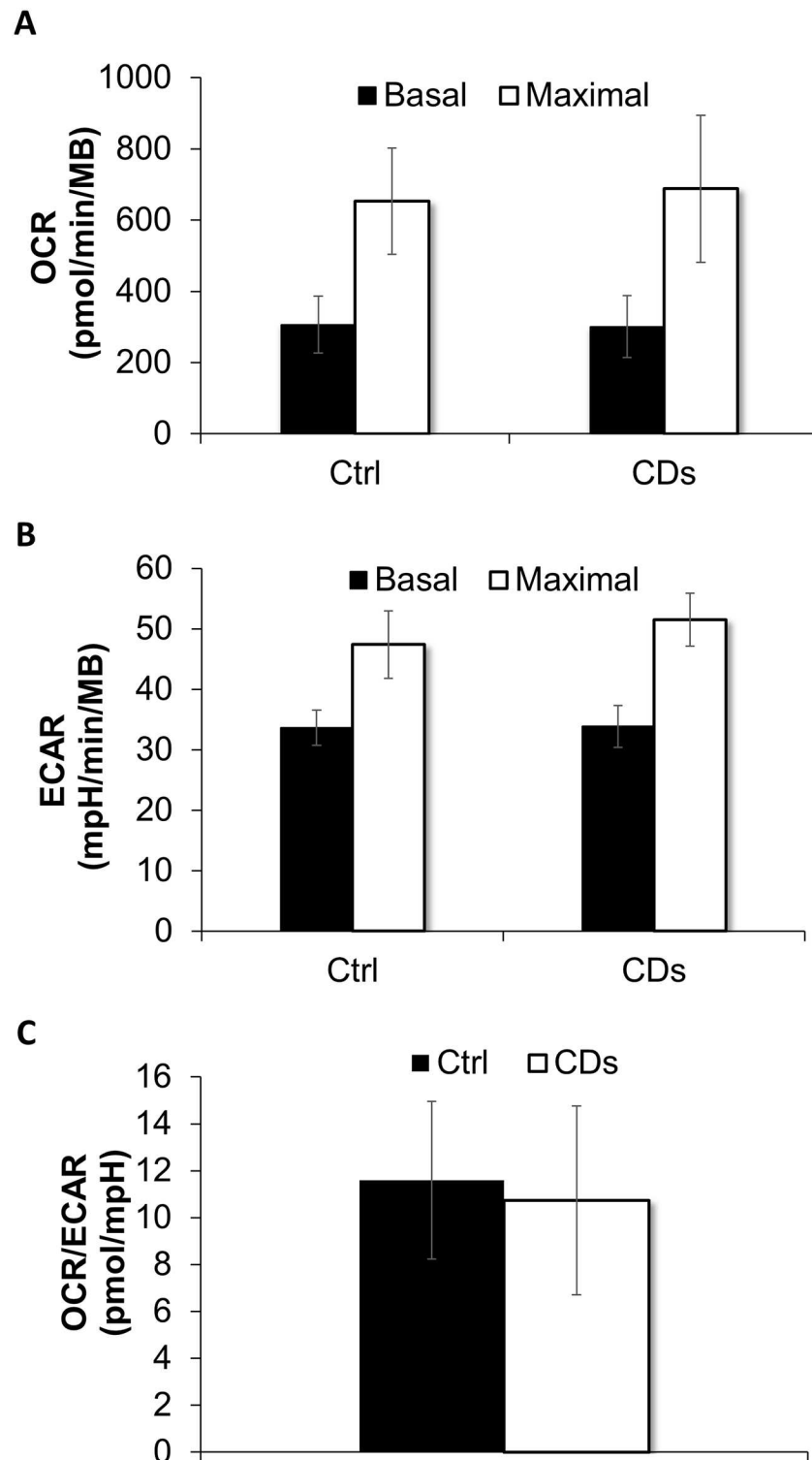
Fig 4. OCR and ECAR. (A) Basal and maximal OCR levels. Basal OCR was measured before Oligomycin injection and maximum OCR after FCCP injection, subtracted by non-mitochondrial respiration (measurement after rotenone and Antimycin A injection). (B) Basal and maximal ECAR levels. Basal ECAR was measured before Oligomycin injection and maximal ECAR levels were measured after the injection of Oligomycin. (C) OCR/ECAR ratio under basal conditions. All OCR and ECAR values were normalized to cell biomass measured by methylene blue (MB). Analysis was performed in five replicate wells for each fibroblast line. Data are mean ± S.E.

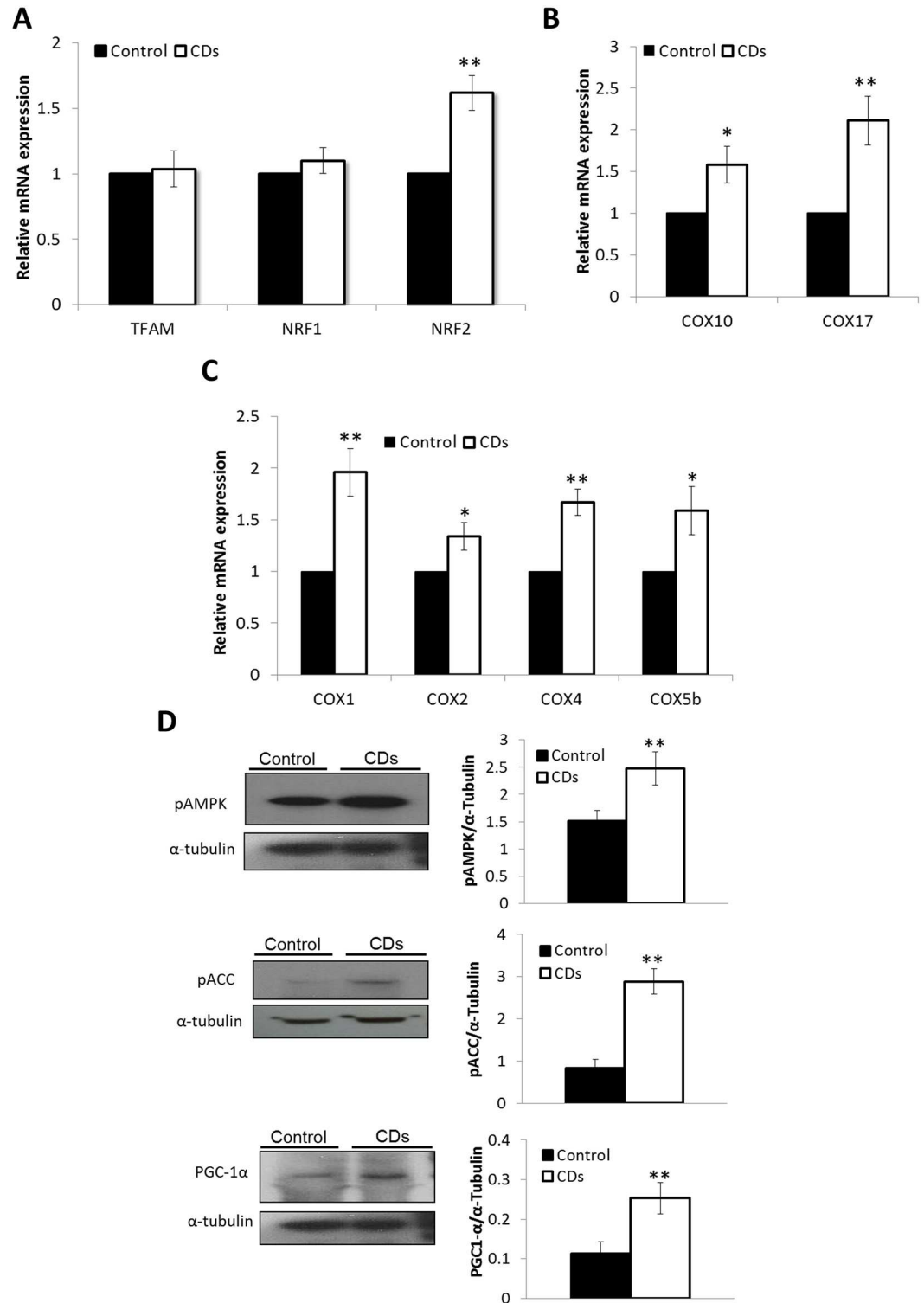doi:10.1371/journal.pone.0165417.g004

Fig 5. Mitochondrial biogenesis. (A) Relative mRNA-expression of mitochondrial-biogenesis related genes. (B) Relative mRNA-expression of COX subunits. (C) Relative mRNA-expression of COX chaperones. (D) Western-blot analysis of pAMPK, pACC and PGC1-α. On the right panel, band intensity ratios relative to α-Tubulin are shown. Western blots images are representative of 3 independent experiments. Gene expression is shown as fold change of expression relative to control fibroblasts. Data are mean ± S.E. (n = 3). *p<0.05, **p<0.01.

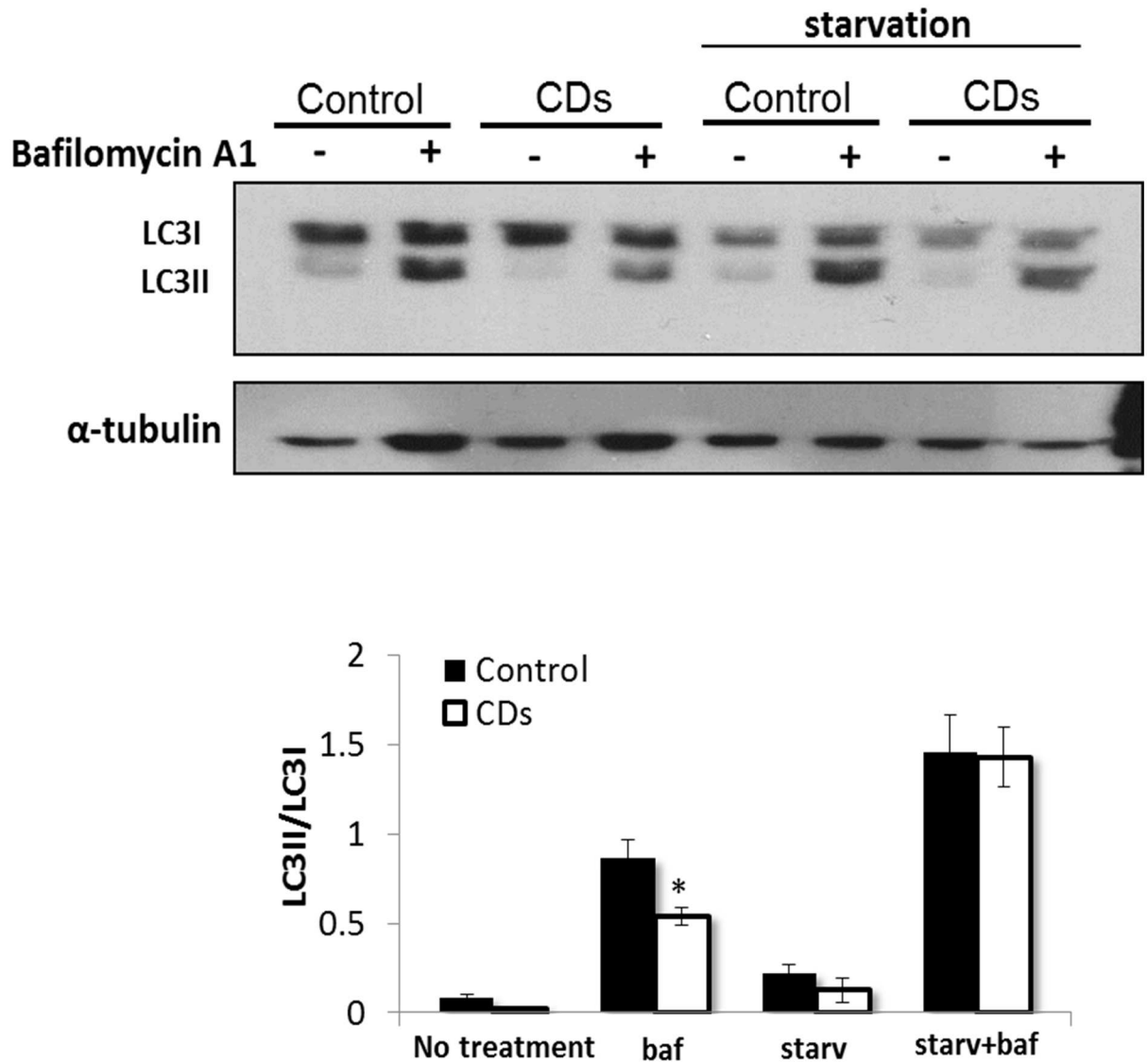doi:10.1371/journal.pone.0165417.g005

Fig 6. Autophagy analysis. Western-blot analysis of LC3-I and LC3-II. Fibroblasts were grown under normal or starvation (starv) conditions in the presence or absence of autophagy inhibitor bafilomycin A1 (baf, 100 nM) for 4 h as described under materials and methods. Lower panel shows the band intensity ratio of LC3-II to LC3-I. Data represent mean ± S.E. of three independent experiments. *$p < 0.05$.

doi:10.1371/journal.pone.0165417.g006

Discussion

Here we demonstrate a decreased COX activity associated with fragmented mitochondria, enhanced ROS production and reduced mitochondrial membrane potential in primary fibroblasts derived from CDs rats. Interestingly, mitochondrial content was upregulated as were markers for mitochondrial biogenesis, probably representing an attempt to compensate for COX-deficiency, thus providing a possible explanation for the unexpectedly intact ATP levels in fibroblasts of the CDs.

The increase in mitochondrial mass observed in the CDs fibroblasts could be due to increased mitochondrial biogenesis, decreased mitochondrial clearance by autophagy or both. Increased mitochondrial biogenesis is a common observation in tissues of patients with
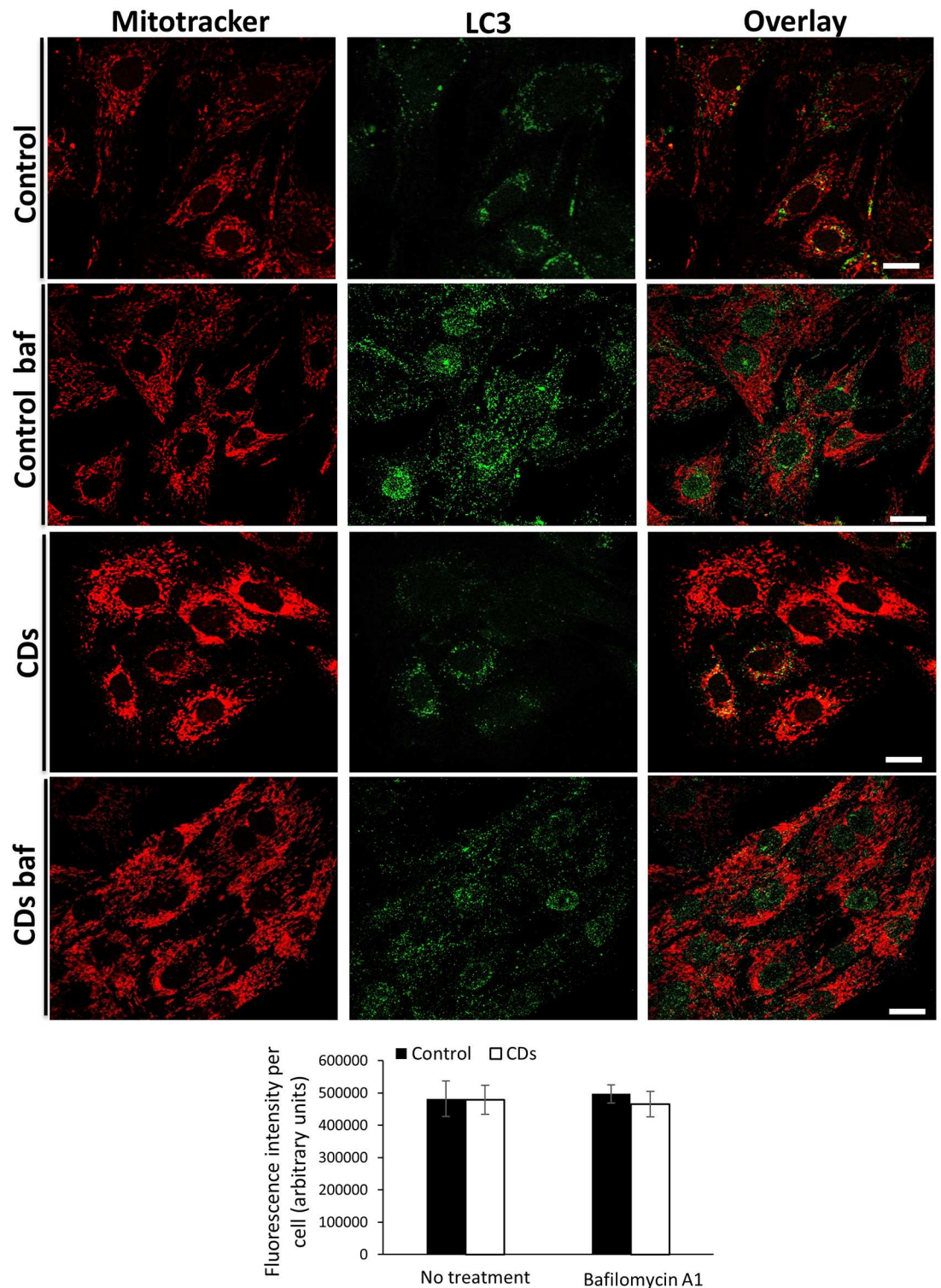
Fig 7. Mitophagy analysis. Co-staining with Mitotracker Red and anti-LC3 antibody in the presence or absence of autophagy inhibitor Bafilomycin A1. The upper panels shows the control fibroblasts and the lower panels the CDs fibroblasts. Below is shown quantitative analysis of fluorescence intensity (arbitrary units) of LC3 and MitoTracker Red co-localization per cell. Data represent mean ± S.E. of three independent experiments. Scale bar, 10 μm.

doi:10.1371/journal.pone.0165417.g007

mitochondrial dysfunction and is assumed to be a compensatory mechanism triggered by the OXPHOS defect [27–29]. However, with regard to COX-deficiency, this has been hardly documented. In the current study, we demonstrated a 50% reduction in COX activity in the CDs fibroblasts, followed by a 2-fold increase in mitochondrial content. We hypothesized that the increase in mitochondrial content in cells of the CDs is the result of increased mitochondrial biogenesis that might be mediated through activation of AMPK, a major regulator of mitochondrial biogenesis, triggered by phosphorylation at threonine-172 [30,31]. Upon activation, phosphorylated AMPK (pAMPK) acts simultaneously on boosting mitochondrial energy production and inhibiting ATP consuming processes [32]. Using Western-blot analysis, we demonstrated elevated pAMPK levels in fibroblasts of the CDs. Accordingly, the protein levels of pAMPK downstream key-targets, PGC-1α and pACC were also markedly increased, supporting AMPK activation. Our findings are consistent with studies showing elevated pAMPK levels in skeletal-muscle of COX-defective mouse models [33]. The relative expression levels of the transcription factor NRF1, which promotes mitochondrial function and biogenesis [20] were unchanged, whereas the expression of several NRF1 immediate target genes including COX1, COX2, COX4, COX5b, COX10 and COX17 were all upregulated in fibroblasts of the CDs. These findings in the CDs are fully compatible with the role of PGC-1α as a transcription coactivator increasing the transcriptional activity of NRF1. To test if the observed enhanced mitochondrial staining in the CDs fibroblasts could be due to mitochondrial accumulation caused by aberrant autophagy clearance, we monitored the endogenous levels of autophagy marker LC3-II [21]. The observation that only low LC3-II levels were found in CDs fibroblasts grown under normal conditions suggested that basal autophagy was not elevated. Autophagy was efficiently induced in starved CDs fibroblasts as demonstrated by the comparable increase in both LC3-II levels and the LC3-II/LC3-I ratio in CDs and control fibroblasts. Moreover, the similar increase in LC3-II levels and the LC3-II/LC3-I ratio following a specific inhibition of autophagy by bafilomycin A1 in both CDs and the control fibroblasts, further support normal autophagic-flux. To reinforce our findings we examined whether the mitochondrial fragments in cells of CDs were associated with LC3 but could not detect any difference in LC3 subcellular localization to the mitochondria between the CDs and the control fibroblasts. These observations might indicate no major autophagy impairment or enhanced autophagic mitochondrial elimination in the CDs fibroblasts, supporting the notion that upregulation of mitochondrial content in the CDs might be due to mitochondrial biogenesis activation. This could reflect cellular attempts to compensate for COX-deficiency in order to prevent energy stress, possibly mediated by the AMPK pathway.

Fibroblasts in culture generate most of their ATP via glycolysis and not by OXPHOS [34,35]. The DMEM-Gal, containing galactose instead of glucose as a carbon source, does not support glycolysis, thus forcing cells to use the mitochondrial OXPHOS to produce ATP. Thereby, fibroblasts having OXPHOS defects are highly sensitive to the DMEM-Gal [36–38]. We have shown that the CDs fibroblasts exhibited reduced cell biomass on DMEM-Gal compared to the control fibroblasts and to the CDs glucose-grown cells, suggesting they primarily rely on glycolysis for energy production. In agreement with the microscopic findings showing increased mitochondrial-staining in the CDs-fibroblasts, quantitative measurement of Mito-Tracker Green stained cells, a dye that binds to mitochondria regardless of their membrane potential, also demonstrated increased mitochondrial content in the CDs-fibroblasts on both the glucose and galactose medium. Moreover, both cellular OCR, resulting from oxidative phosphorylation, and ECAR, associated with glycolytic metabolism as well as the OCR/ECAR ratio were intact in the CDs fibroblasts. These results indicates that the COX defect was not sufficient to reduce oxygen consumption, likely due to the increase in mitochondrial mass, and does not support the occurrence of a shift from OXPHOS towards a glycolytic state. However, mitochondrial membrane potential and the ATP levels per mitochondria in CDs-fibroblasts

were decreased. Yet, the cellular ATP levels in the CDs fibroblasts were unchanged in either the glucose or galactose media. We propose that these conflicting results could be the outcome of an adaptive cellular response to the metabolic environment attempting to overcome COX defect by increasing mitochondrial biomass. Following our assumption, the CDs fibroblast maintained unchanged total cellular-ATP level though ATP levels per mitochondria were reduced, as a consequence of the increase in mitochondria content triggered by reduction in COX activity and in mitochondrial membrane potential. Yet, this compensatory mechanism was not observed in islets and could be specific to the fibroblasts [12].

Mitochondria are one of the major cellular sources of ROS and mitochondrial dysfunction often leads to ROS overproduction. Indeed, in the current study, fibroblasts of the CDs exhibited increased ROS production on DMEM-Glu, enhancing remarkably on DMEM-Gal, possibly due to COX-dysfunction and the increased mitochondrial mass. Our findings are consistent with previous observations showing elevated ROS levels in COX-deficient fibroblasts [39]. Supporting an increase in oxidative stress, we found the expression of the transcription factor NRF2, that facilitate cellular antioxidant response to oxidative stress [40] to be upregulated in fibroblasts of CDs rats. The cellular role of mitochondria is reflected by their structure. In accordance, the CDs-fibroblasts displayed altered mitochondrial morphology including pronounced fragmentation and perinuclear clustering compared to the elongated filamentous mitochondria observed in the control fibroblasts. Similarly, others have also shown that treating cells with COX inhibitor KCN induced mitochondrial fragmentation [41]. Punctate mitochondrial appearance was also observed in samples from respiratory complex I and multi-complex deficient patients [34] and several studies showed that inhibition of mitochondrial respiratory complexes I–V induced mitochondrial fragmentation in human skin fibroblasts [41–44]. These may suggest a crosstalk between mitochondrial dysfunction and mitochondrial morphology in which changes in mitochondrial morphology could reflect alterations in energy metabolism.

Our data suggest that COX dysfunction in the CDs fibroblasts triggers upregulation of mitochondrial content due to the stimulation of mitochondrial biogenesis rather than impaired autophagic clearance. This is likely to occur by activation of the AMPK-dependent pathway, thereby counteracting the detrimental effect of COX-deficiency thus allowing the CDs fibroblasts to maintain overall ATP levels unaffected.

Acknowledgments

Author Contributions

Conceptualization: AKL SWZ.

Investigation: AKL SWZ AS.

Methodology: AKL SWZ AS DS LD GL.

Resources: SWZ IR.

Writing – original draft: AKL SWZ AS GL DS IR.

Writing – review & editing: AKL SWZ AS GL DS IR.

References

1. Brunori M, Wilson MT. Electron transfer and proton pumping in cytochrome oxidase. Biochimie 1995 Jan; 77(7–8):668–76.

2. Calhoun MW, Thomas JW, Gennis RB. The cytochrome oxidase superfamily of redox-driven proton pumps. Trends Biochem Sci 1994 Aug; 19(8):325–30. PMID: 7940677 doi: 10.1016/0968-0004(94)90071-X

3. Hatefi Y. The mitochondrial electron transport and oxidative phosphorylation system. Annu Rev Biochem 1985 Jan; 54:1015–69. PMID: 2862839 doi: 10.1146/annurev.bi.54.070185.005055

4. Willis JH, Capaldi RA, Huigsloot M, Rodenburg RJT, Smeitink J, Marusich MF. Isolated deficiencies of OXPHOS complexes I and IV are identified accurately and quickly by simple enzyme activity immuno-capture assays. Biochim Biophys Acta 2009 May; 1787(5):533–8. PMID: 19041632 doi: 10.1016/j.bbabio.2008.10.009

5. Paradies G, Ruggiero FM, Petrosillo G, Quagliariello E. Age-dependent decrease in the cytochrome c oxidase activity and changes in phospholipids in rat-heart mitochondria. Arch Gerontol Geriatr Jan; 16 (3):263–72. PMID: 15374339 doi: 10.1016/0167-4943(93)90037-I

6. Sohal RS. Aging, cytochrome oxidase activity, and hydrogen peroxide release by mitochondria. Free Radic Biol Med 1993 Jun; 14(6):583–8. PMID: 8392019 doi: 10.1016/0891-5849(93)90139-L

7. Saada A. Mitochondria: mitochondrial OXPHOS (dys) function ex vivo—the use of primary fibroblasts. Int J Biochem Cell Biol 2014 Mar; 48:60–5. PMID: 24412346 doi: 10.1016/j.biocel.2013.12.010

8. Abdulhag UN, Soiferman D, Schueler-Furman O, Miller C, Shaag A, Elpeleg O, et al. Mitochondrial complex IV deficiency, caused by mutated COX6B1, is associated with encephalomyopathy, hydrocephalus and cardiomyopathy. Eur J Hum Genet 2014 Apr; 23(2):159–64. PMID: 24781756 doi: 10.1038/ejhg.2014.85

9. Diaz F. Cytochrome c oxidase deficiency: Patients and animal models. Biochim Biophys Acta—Mol Basis Dis 2010 Jan; 1802(1):100–10. PMID: 19682572 doi: 10.1016/j.bbadis.2009.07.013

10. De Paepe B, Smet J, Vanlander A, Seneca S, Lissens W, De Meirleir L, et al. Fluorescence imaging of mitochondria in cultured skin fibroblasts: a useful method for the detection of oxidative phosphorylation defects. Pediatr Res 2012 Sep; 72(3):232–40. PMID: 22728747 doi: 10.1038/pr.2012.84

11. Weksler-Zangen S, Yagil C, Zangen DH, Ornoy A, Jacob HJ, Yagil Y. The newly inbred cohen diabetic rat: a nonobese normolipidemic genetic model of diet-induced type 2 diabetes expressing sex differences. Diabetes 2001 Nov; 50(11):2521–9. PMID: 11679430 doi: 10.2337/diabetes.50.11.2521

12. Weksler-Zangen S, Aharon-Hananel G, Mantzur C, Aouizerat T, Gurgul-Convey E, Raz I, et al. IL-1β hampers glucose-stimulated insulin secretion in Cohen diabetic rat islets through mitochondrial cytochrome c oxidase inhibition by nitric oxide. Am J Physiol Endocrinol Metab 2014 Mar; 306(6):E648–57. PMID: 24425765 doi: 10.1152/ajpendo.00451.2013

13. Weksler-Zangen S, Jorns A, Tarsi-Chen L, Vernea F, Aharon-Hananel G, Saada A, et al. Dietary copper supplementation restores beta-cell function of Cohen diabetic rats: a link between mitochondrial function and glucose-stimulated insulin secretion. Am J Physiol Endocrinol Metab 2013 Mar; 304(10): E1023–34. PMID: 23512809 doi: 10.1152/ajpendo.00036.2013

14. Ornoy A, Tsadok MA, Yaffe P, Zangen SW. The Cohen diabetic rat as a model for fetal growth restriction: vitamins C and E reduce fetal oxidative stress but do not restore normal growth. Reprod Toxicol 2009 Dec; 28(4):521–9. PMID: 19539026 doi: 10.1016/j.reprotox.2009.06.005

15. Saada A, Bar-Meir M, Belaiche C, Miller C, Elpeleg O. Evaluation of enzymatic assays and compounds affecting ATP production in mitochondrial respiratory chain complex I deficiency. Anal Biochem 2004 Dec; 335(1):66–72. PMID: 15519572 doi: 10.1016/j.ab.2004.08.015

16. Golubitzky A, Dan P, Weissman S, Link G, Wikstrom JD, Saada A. Screening for active small molecules in mitochondrial complex I deficient patient's fibroblasts, reveals AICAR as the most beneficial compound. PLoS One 2011 Jan; 6(10):e26883. PMID: 22046392 doi: 10.1371/journal.pone.0026883

17. Kukidome D, Nishikawa T, Sonoda K, Imoto K, Fujisawa K, Yano M, et al. Activation of AMP-activated protein kinase reduces hyperglycemia-induced mitochondrial reactive oxygen species production and promotes mitochondrial biogenesis in human umbilical vein endothelial cells. Diabetes 2006 Jan; 55 (1):120–7. PMID: 16380484 doi: 10.2337/diabetes.55.01.06.db05-0943

18. Lowry OH, Rosebrough NJ, Farr AL, Randall RJ. Protein measurement with the Folin phenol reagent. J Biol Chem 1951 Nov; 193(1):265–75. PMID: 14907713.

19. Pendergrass W, Wolf N, Poot M. Efficacy of MitoTracker Green and CMXrosamine to measure changes in mitochondrial membrane potentials in living cells and tissues. Cytometry A 2004 Oct; 61 (2):162–9. PMID: 15382028 doi: 10.1002/cyto.a.20033

20. Scarpulla RC. Nuclear control of respiratory gene expression in mammalian cells. J Cell Biochem 2006 Mar; 97(4):673–83. PMID: 16329141 doi: 10.1002/jcb.20743

21. Mizushima N, Yoshimori T. How to interpret LC3 immunoblotting. Autophagy Jan; 3(6):542–5. PMID: 17611390 doi: 10.4161/auto.4600

22. Kabeya Y, Mizushima N, Ueno T, Yamamoto A, Kirisako T, Noda T, et al. LC3, a mammalian homologue of yeast Apg8p, is localized in autophagosome membranes after processing. EMBO J 2000 Nov; 19(21):5720–8. PMID: 11060023 doi: 10.1093/emboj/19.21.5720

23. Yamamoto A, Tagawa Y, Yoshimori T, Moriyama Y, Masaki R, Tashiro Y. Bafilomycin A1 prevents maturation of autophagic vacuoles by inhibiting fusion between autophagosomes and lysosomes in rat hepatoma cell line, H-4-II-E cells. Cell Struct Funct 1998 Feb; 23(1):33–42. PMID: 9639028 doi: 10.1247/csf.23.33

24. Mijaljica D, Prescott M, Devenish RJ. Mitophagy and mitoptosis in disease processes. Methods Mol Biol 2010 Jan; 648:93–106. PMID: 20700707 doi: 10.1007/978-1-60761-756-3_6

25. Dagda RK, Zhu J, Kulich SM, Chu CT. Mitochondrially localized ERK2 regulates mitophagy and autophagic cell stress: implications for Parkinson's disease. Autophagy 2008 Aug; 4(6):770–82. PMID: 18594198 doi: 10.4161/auto.6458

26. Rodriguez-Enriquez S, Kim I, Currin RT, Lemasters JJ. Tracker dyes to probe mitochondrial autophagy (mitophagy) in rat hepatocytes. Autophagy 2006 Jan; 2(1):39–46. PMID: 16874071 doi: 10.4161/auto.2229

27. Rossmanith W, Freilinger M, Roka J, Raffelsberger T, Moser-Thier K, Prayer D, et al. Isolated cytochrome c oxidase deficiency as a cause of MELAS. J Med Genet 2008 Feb; 45(2):117–21. PMID: 18245391 doi: 10.1136/jmg.2007.052076

28. DiMauro S, Schon EA. Mitochondrial respiratory-chain diseases. N Engl J Med 2003 Jun; 348 (26):2656–68. PMID: 12826641 doi: 10.1056/NEJMra022567

29. Giordano C, Iommarini L, Giordano L, Maresca A, Pisano A, Valentino ML, et al. Efficient mitochondrial biogenesis drives incomplete penetrance in Leber's hereditary optic neuropathy. Brain 2014 Feb; 137 (Pt 2):335–53. PMID: 24369379 doi: 10.1093/brain/awt343

30. Reznick RM, Shulman GI. The role of AMP-activated protein kinase in mitochondrial biogenesis. J Physiol. 2006 Jul; 574(1):33–9. PMID: 16709637 doi: 10.1113/jphysiol.2006.109512

31. Kahn BB, Alquier T, Carling D, Hardie DG. AMP-activated protein kinase: ancient energy gauge provides clues to modern understanding of metabolism. Cell Metab 2005 Jan; 1(1):15–25. PMID: 16054041 doi: 10.1016/j.cmet.2004.12.003

32. Hardie DG. The AMP-activated protein kinase pathway—new players upstream and downstream. J Cell Sci 2004 Nov; 117(Pt 23):5479–87. PMID: 15509864 doi: 10.1242/jcs.01540

33. Viscomi C, Bottani E, Civiletto G, Cerutti R, Moggio M, Fagiolari G, et al. In vivo correction of COX deficiency by activation of the AMPK/PGC-1α axis. Cell Metab 2011 Jul; 14(1):80–90. PMID: 21723506 doi: 10.1016/j.cmet.2011.04.011

34. Benard G, Bellance N, James D, Parrone P, Fernandez H, Letellier T, et al. Mitochondrial bioenergetics and structural network organization. J Cell Sci 2007 Mar; 120(Pt 5):838–48. PMID: 17298981 doi: 10.1242/jcs.03381

35. Rossignol R, Gilkerson R, Aggeler R, Yamagata K, Remington SJ, Capaldi RA. Energy substrate modulates mitochondrial structure and oxidative capacity in cancer cells. Cancer Res 2004 Feb; 64 (3):985–93. PMID: 14871829 doi: 10.1158/0008-5472.CAN-03-1101

36. Enríquez JA, Cabezas-Herrera J, Bayona-Bafaluy MP, Attardi G. Very rare complementation between mitochondria carrying different mitochondrial DNA mutations points to intrinsic genetic autonomy of the organelles in cultures human cells. J Biol Chem 2000 Apr 14; 275(15):11207–15. PMID: 10753928 doi: 10.1074/jbc.275.15.11207

37. Robinson BH, Petrova-Benedict R, Buncic JR, Wallace DC. Nonviability of cells with oxidative defects in galactose medium: a screening test for affected patient fibroblasts. Biochem Med Metab Biol 1992 Oct; 48(2):122–6. PMID: 1329873 doi: 10.1016/0885-4505(92)90056-5

38. Auré K, Mamchaoui K, Frachon P, Butler-Browne GS, Lombès A, Mouly V. Impact on oxidative phosphorylation of immortalization with the telomerase gene. Neuromuscul Disord 2007 May; 17(5):368–75. PMID: 17383182 doi: 10.1016/j.nmd.2007.01.019

39. Soiferman D, Ayalon O, Weissman S, Saada A. The effect of small molecules on nuclear-encoded translation diseases. Biochimie 2014 May; 100:184–91. PMID: 24012549 doi: 10.1016/j.biochi.2013.08.024

40. Ma Q. Role of Nrf2 in Oxidative Stress and Toxicity. Annu Rev Pharmacol Toxicol 2013 Jan; 53 (1):401–26. PMID: 23294312 doi: 10.1146/annurev-pharmtox-011112-140320

41. Guillery O, Malka F, Frachon P, Milea D, Rojo M, Lombès A. Modulation of mitochondrial morphology by bioenergetics defects in primary human fibroblasts. Neuromuscul Disord 2008 Apr; 18(4):319–30. PMID: 18395446 doi: 10.1016/j.nmd.2007.12.008

42. Pham NA, Richardson T, Cameron J, Chue B, Robinson BH. Altered Mitochondrial Structure and Motion Dynamics in Living Cells with Energy Metabolism Defects Revealed by Real Time Microscope Imaging. Microsc Microanal 2004 Mar; 10(02):247–60. PMID: 15306050 doi: 10.1017/S143192760404005X

43. Liot G, Bossy B, Lubitz S, Kushnareva Y, Sejbuk N, Bossy-Wetzel E. Complex II inhibition by 3-NP causes mitochondrial fragmentation and neuronal cell death via an NMDA- and ROS-dependent pathway. Cell Death Differ 2009 Jun; 16(6):899–909. PMID: 19300456 doi: 10.1038/cdd.2009.22

44. Westermann B. Bioenergetic role of mitochondrial fusion and fission. Biochim Biophys Acta 2012 Oct; 1817(10):1833–8. PMID: 22409868 doi: 10.1016/j.bbabio.2012.02.033